ELSEVIER

Journal of Nuclear Materials 282 (2000) 54–65

journal of nuclear materials

www.elsevier.nl/locate/jnucmat

Sintering studies on UO_2–PuO_2 pellets with varying PuO_2 content using dilatometry

T.R.G. Kutty *, P.V. Hegde, K.B. Khan, S. Majumdar, D.S.C. Purushotham

Radiometallurgy Division, Bhabha Atomic Research Centre, Trombay, Mumbai 400 085, India

Received 23 October 1999; accepted 18 July 2000

Abstract

The sintering behaviour of UO_2, PuO_2, UO_2–20%PuO_2, UO_2–50%PuO_2 and UO_2–76%PuO_2 pellets have been studied using a dilatometer in inert, reducing and oxidizing atmospheres. The onset of shrinkage occurs by about 400°C lower in oxidizing atmosphere such as CO_2 and commercial N_2 than that occurs in reducing atmosphere. PuO_2 and UO_2–76%PuO_2 showed an expansion on heating in Ar at ~1000°C. UO_2–20%PuO_2 pellet sinters slightly better in Ar than in Ar–8%H_2. From the shrinkage rate curves, it was found that the maximum shrinkage rate occurs in commercial nitrogen atmosphere for UO_2–50%PuO_2. For the other compositions, the maximum shrinkage rate was observed for Ar atmosphere. The sintering behaviour of above mentioned pellets was discussed with the help of point defect model and the possible mechanisms were suggested.

PACS: 61.72.−y; 81.20.Ev; 66.30. Fq

1. Introduction

The established fabrication route for large scale production of mixed uranium plutonium oxide fuel pellets is cold compaction followed by high temperature sintering in reducing atmosphere at around 1650°C. The mixed oxide fuel for fast reactors is usually fabricated with an O/M ratio of around 1.95 in order to achieve better compatibility between fuel, clad and coolant [1]. To get a stoichiometry of around 1.95, it is necessary to maintain a reducing atmosphere in the sintering furnace, such as H_2 or Ar–H_2 mixture, so that the H_2O/H_2 ratio in the reducing zone of the sintering furnace is always $<10^{-2}$ [2,3]. There are several parameters that influence the H_2O/H_2 ratio in the atmosphere of furnace which are listed below [3]:

(a) H_2O/H_2 ratio of the sintering gas at the inlet side of the furnace;

(b) H_2O evolution by the reduction of UO_{2+x} and PuO_2;

(c) O/M ratio of the starting powders.

During the fabrication of mixed oxide fuel under reducing condition, the oxygen potential is not generally controlled, which is generally in the range from −30 to −120 kcal/mol, typical for dry H_2 [4]. The point defect model predicts a small vacancy concentration in slightly hypostoichiometric oxide. The value of cation diffusion coefficient under such conditions is near to the observed minimum [5]. Even at 1700°C, mean interdiffusion distances during sintering even for 4 h are of the order of 0.1–0.5 μm and therefore negligible [4]. Therefore, homogenization and formation of a solid solution are not achieved in normal reducing atmosphere. This results in a two phased microstructure with one phase being richer in Pu. This Pu rich zone may produce hot spots during the reactor operation and cause difficulties in the dissolution step of reprocessing [6]. Achieving homogenization and complete solid solution of UO_2–PuO_2 powders is therefore a technologically important problem. A change in the sintering atmosphere from reducing to oxidizing conditions has been reported to increase the interdiffusion rates [7]. Cation mobility increases drastically in hyperstoichiometric oxide because of the large

* Corresponding author. Tel.: +91-22 550 5319; fax: +91-22 550 5151.

E-mail address: tkutty@magnum.barc.ernet.in (T.R.G. Kutty).

0022-3115/00/$ - see front matter
PII: S0022-3115(00)00394-9

increase in cation vacancy concentration [8]. A low temperature short time sintering has been developed to take advantage of the very high cation mobilities in hyperstoichiometric oxides. Sintering rate under oxidizing conditions with the associated fast diffusion can be better in a short time below 1300°C rather than in a longer time at 1650°C for reducing atmospheres. This process results in large scale savings in energy, time and capital investment [7]. However, there is a requirement for a reduction step to achieve the necessary O/M ratio (~1.95) which would partially offset the above mentioned advantages.

In this work, the shrinkage behaviour of UO_2, UO_2–20%PuO_2, UO_2–50%PuO_2, UO_2–76%PuO_2 and PuO_2 pellets were studied using a dilatometer in different types of inert, reducing and oxidizing atmospheres. UO_2–20%PuO_2 is a well-established fuel for fast breeder reactors. UO_2–50%PuO_2 and UO_2–76%PuO_2 have been considered as possible alternate fuels for Indian Fast Breeder Test Reactor (FBTR). The Pu-rich oxide fuel could be used as a fuel for compact fast reactors as a substitute for the highly enriched uranium (HEU). So far, studies have not been reported on above mentioned compositions in a wide range of atmospheres like Ar, Ar–8%H_2, CO_2 and commercial N_2. Hence, it is felt that the results of this study would be useful to the manufacturers of such fuels.

1.1. U–Pu–O system

Both UO_2 and PuO_2 crystallize in fluorite type structure with lattice parameters of 0.5468 nm and 0.5396 nm, respectively. On the basis of isomorphism and a very small difference in the ionic size between the two, one would expect to have a continuous series of solid solution between the two components. The single phase field of UO_2 exists only at about 2500°C from O/U 1.65–2.25 [1,9]. At low temperature, UO_{2+x} and U_4O_{9-y} phase coexists in the range of O/M 2–2.25. The hypostoichiometric UO_2 exists only at very high temperature whereas hyperstoichiometric oxide exists even at very low temperature. Up to 300°C, PuO_{2-x} and $PuO_{1.52}$ phase is stable within O/Pu ratio of 1.52–2.0. Above that temperature PuO_{2-x} and $PuO_{1.61}$ phases are in equilibrium within O/Pu ratio of 1.61–2.0 [10,11]. The stoichiometric PuO_2 can be made hypostoichiometric by heating in reducing/inert atmosphere. UO_2 can dissolve large amount of interstitial oxygen to form anion excess UO_{2+x}, while PuO_2 or (U,Pu)O_2 can accommodate large amount of oxygen vacancies in their lattice. (U,Pu)O_2 can be made hypostoichiometric very easily by reducing Pu^{+4} to Pu^{+3}, with the charge compensation by the introduction of oxygen vacancies. The charge compensation for the excess of oxygen in UO_{2+x} is achieved by oxidizing U^{+4}–U^{+5} [12]. It is well known that at larger x-values, cluster formation occurs. The basic unit of a cluster in MO_{2-x} is of the type Pu^{3+}–V_O–Pu^{3+}, where V_O is the oxygen vacancy [1,7]. These clusters can grow stepwise by doubling or trebling, etc. their size.

U–Pu–O ternary system for a range of O/M ratio between 1.5 and 2.7 at 200°C is shown in Fig. 1 [13]. It can be seen that for low Pu content i.e., <30%PuO_2, $MO_{2\pm x}$ exists for a wide range of O/M. For the UO_2 rich composition and for high O/M ratio (>2), the M_4O_9 and MO_{2+x} phase co-exists. At still higher O/M ratio of 2.3 and above, M_4O_9 phase is present with M_3O_8. For the PuO_2 rich end, MO_2 phase exists only at an O/M ratio of 2.0. Below this value, for high PuO_2 composition, a two phase region is noticed which comprises of MO_{2-x} and α-M_2O_3 [14]. It can be seen from Fig. 1 that $MO_{2\pm x}$ is the most predominant phase which exists for a wide range of composition and O/M ratio.

2. Experimental

2.1. Fabrication of green pellet

The green pellets for this study were prepared by the conventional powder metallurgy technique involving mixing and cold compaction. The UO_2 and PuO_2 powders were milled for 4 h in a planetary ball mill using

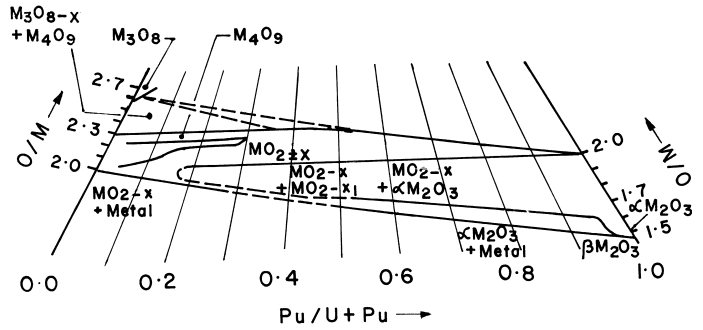

Fig. 1. U–Pu–O ternary system for a range of O/M ratio between 1.5 and 2.7 at 200°C [13].

Table 1
Characteristics of UO_2 and PuO_2 powders

Property	UO_2	PuO_2
Oxygen to metal ratio	2.10	2.00
Apparent density (g/cm^3)	1.5	1.2
Total impurities (ppm)	<800	<1200
Specific surface area (m^2/g)	2.8	13.6
Theoretical density (g/cm^3)	10.96	11.46

tungsten carbide balls. The blended powder was precompacted, granulated and finally compacted at around 300 MPa to green pellets of 4.6 mm diameter and around 8 mm in length. The density of green pellets was $52 \pm 1\%$ of theoretical density (TD). To facilitate compaction and to impart handling strength to the green pellets, 1 wt% zinc behenate was added as lubricant/binder during the last hour of milling. The characteristics of UO_2 and PuO_2 powders used in this study is given in Table 1.

2.2. Dilatometry

The shrinkage behaviour of the UO_2, UO_2–20%PuO_2, UO_2–50%PuO_2, UO_2–76%PuO_2 and PuO_2 compacts in the various atmospheres was studied using a push rod type dilatometer. The shrinkage was measured in axial direction. The sample supporter, measuring unit and displaceable furnace of the dilatometer were mounted horizontally as shown in Fig. 2. The length change measurements were made by an LVDT transducer which was maintained at a constant temperature by means of water circulation from a constant temperature bath. The accuracy of the measurement of change in length was within ± 0.1 μm. The temperature was measured using a calibrated thermocouple which is placed directly above the sample. A small force of 0.2 N was applied to the sample through the push rod. The dilatometric experiments were carried out using a flow rate of 18 l/h and a heating rate of 6°C/min. The impurity contents of the cover gases used in this study are given in Table 2.

The selection of the temperature programme was controlled by a computer via data acquisition system. Correction was applied to the expansion of the system by taking a run under identical condition using a standard sample (POCO graphite, NIST).

2.3. Characterization

The mixed oxide pellets sintered in different atmospheres were characterized in terms of their density, oxygen to metal ratio (O/M) and phase content. The O/M ratio was measured thermogravimetrically and the phase content was estimated using X-ray diffractometry and metallography. Table 3 gives the typical values of

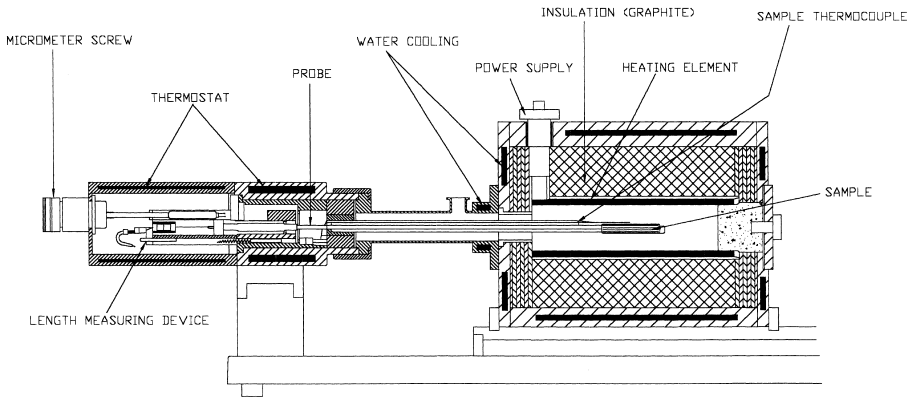

Fig. 2. A schematic of dilatometer showing sample, push rod, themocouple, and LVDT probe.

Table 2
Impurity contents of different sintering atmospheres

Sintering atmosphere	Oxygen (vppm)	Moisture (vppm)	CO_2 (vppm)	CO (vppm)	N_2 (vppm)	Oxides of N_2 (vppm)	Hydrocarbon (vppm)
Argon	4	4	1	1	10	1	1.5
Argon + 8% hydrogen	4	4	1	1	10	1	2
Carbon dioxide	300–400	10	–	5	50	15	2
Commercial nitrogen	400–500	10	50	5	–	–	5

Table 3
Typical values of sintered density, oxygen to metal ratio (O/M) and defect concentrations of UO_2–PuO_2 pellets sintered in various atmospheres

Pellet composition	Sintering atmosphere	Sintered density (%TD)	Oxygen to metal ratio (O/M)	Metal vacancy concentration[a]	Metal interstitial concentration[a]
UO_2	Ar–8%H_2	96	2.0000	4.249E−08	1.1879E−17
	CO_2	96	2.1000	0.4012E−00	8.330E−31
UO_2–20%PuO_2	Ar–8%H_2	94	1.9500	3.801E−14	1.328E−11
	CO_2	95	2.0910	0.332E−00	1.006E−39
UO_2–50%PuO_2	Ar–8%H_2	92	1.8700	5.623E−15	8.977E−11
	CO_2	87	2.0860	0.297E−00	1.126E−30
UO_2–76%PuO_2	Ar–8%H_2	91	1.9400	2.639E−14	1.912E−11
	CO_2	85	2.0754	0.228E−00	1.465E−30
PuO_2	Ar–8%H_2	88	1.9200	1.485E−14	3.399E−11
	CO_2	84	2.0030	3.616E−04	9.256E−28

[a] Details of the calculation of defect concentrations are given in Appendix A.

O/M and their density. The X-ray diffraction patterns of the pellets were obtained by using Cu K_α radiation and graphite monochromator. For metallography, the sintered pellet was mounted in Bakelite and ground using successive grades of emery paper. The final polishing was done using diamond paste.

3. Results

Fig. 3 shows the shrinkage behaviour of UO_2 under various atmospheres. The corresponding shrinkage rates $\mathrm{d}(\mathrm{d}l/l_0)/\mathrm{d}t$ of the above pellet are shown in Fig. 4. Fig. 5 shows shrinkage behaviour of UO_2–20%PuO_2 pellets in different atmospheres such as Ar, Ar–8%H_2, CO_2 and commercial N_2. The corresponding shrinkage rates $(\mathrm{d}(\mathrm{d}l/l_0)/\mathrm{d}t)$ are shown in Fig. 6. Figs. 7–9 illustrate the shrinkage behaviour of UO_2–50%PuO_2, UO_2–

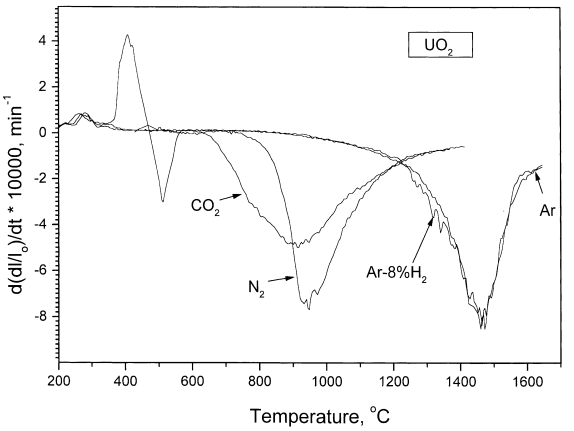

Fig. 4. Shrinkage rate $\mathrm{d}(\mathrm{d}l/l_0)/\mathrm{d}t$ of UO_2 pellet in Ar–8%H_2, Ar, CO_2 and commercial N_2 atmospheres plotted against temperature.

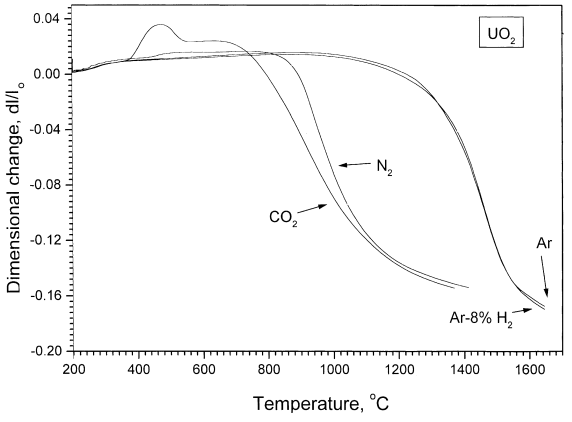

Fig. 3. Shrinkage curves for UO_2 pellets in Ar–8%H_2, Ar, CO_2 and commercial N_2. The $\mathrm{d}l/l_0$ values are plotted against temperature, where l_0 is the initial length.

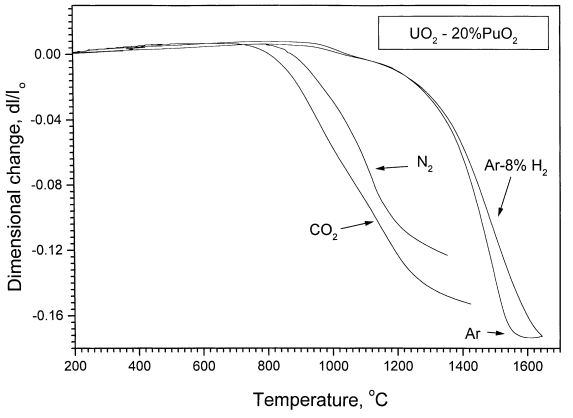

Fig. 5. Shrinkage curves for UO_2–20%PuO_2 pellet in Ar–8%H_2, Ar, CO_2 and commercial N_2.

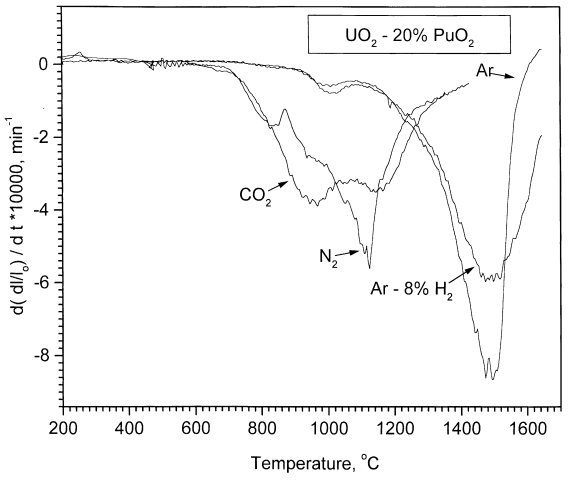

Fig. 6. Shrinkage rate for UO_2–20%PuO_2 pellet in Ar–8%H_2, Ar, CO_2 and commercial N_2 plotted against temperature.

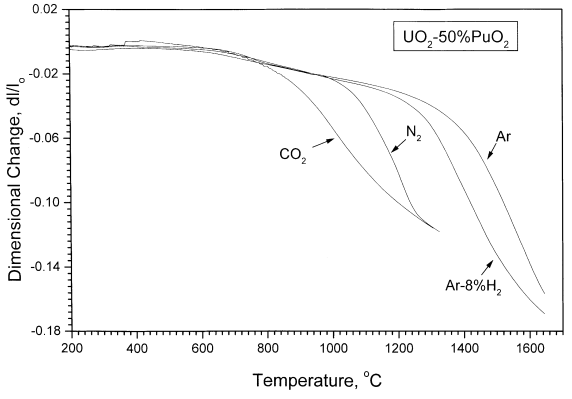

Fig. 7. Shrinkage curves for UO_2–50%PuO_2 in Ar–8%H_2, Ar, CO_2 and commercial N_2 atmospheres.

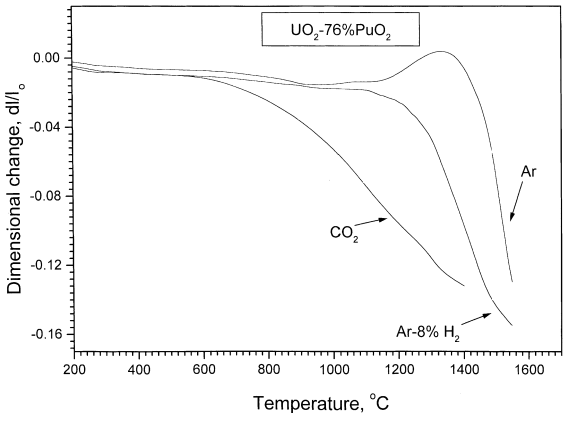

Fig. 8. Shrinkage (dl/l_0) values plotted against temperature for UO_2–76%PuO_2 for different atmospheres.

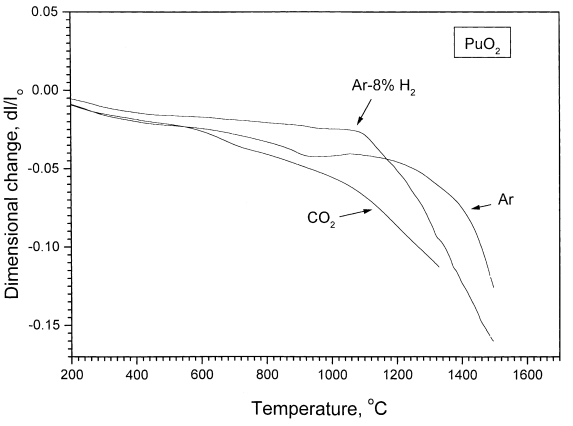

Fig. 9. Shrinkage curves for PuO_2 in Ar–8%H_2, Ar, and CO_2 atmospheres.

76%PuO_2 and PuO_2 pellets. Fig. 10 shows the intercomparison of the shrinkage behaviour of UO_2, UO_2–20%PuO_2, UO_2–50%PuO_2, UO_2–76%PuO_2 and PuO_2 in Ar–8%H_2. Fig. 11 shows the shrinkage curves for the above pellets in CO_2.

It can be seen from Figs. 3–9 that the onset of shrinkage occurs between 600°C and 800°C in CO_2. On the other hand, it begins between 1100 °C and 1200°C in Ar–8%H_2 for UO_2 and UO_2–PuO_2 pellets. In argon, the shrinkage behaviour is almost like that in Ar–8%H_2. The commercial N_2 atmosphere behaves almost like CO_2 except that the shrinkage occurs at a slightly higher temperature for all the compositions (900–1000°C).

It is also noted for UO_2–20%PuO_2, UO_2–50%PuO_2 and UO_2–76%PuO_2, that the sintering rate is retarded in Ar–8%H_2 at around 900–1100°C. For UO_2–76%PuO_2 and PuO_2, an expansion in the shrinkage curve is noted

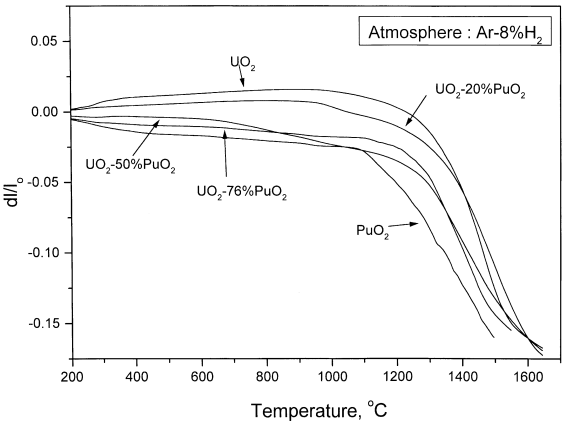

Fig. 10. Intercomparison of the shrinkage behaviour of UO_2, UO_2–20%PuO_2, UO_2–50%PuO_2, UO_2–76%PuO_2 and PuO_2 in reducing atmosphere (Ar–8%H_2).

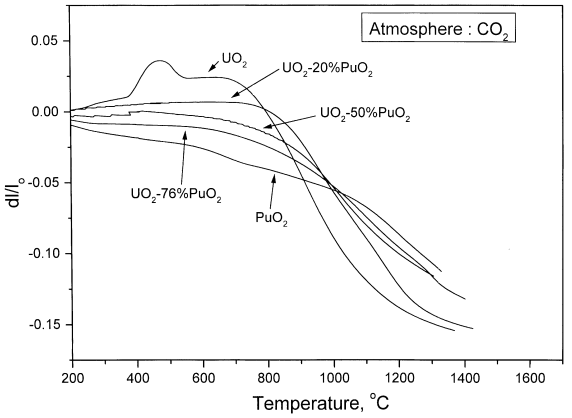

Fig. 11. The shrinkage behaviour of UO_2, UO_2–20%PuO_2, UO_2–50%PuO_2, UO_2–76%PuO_2 and PuO_2 in oxidising atmosphere (CO_2).

at around 1150–1300°C in Ar, the expansion being very predominant for UO_2–76%PuO_2 (see Fig. 8). This expansion is followed by steep shrinkage showing a maximum shrinkage rate of 25 μm/min at 1450°C.

Another interesting phenomenon observed is that, for UO_2, the shrinkage behaviour in Ar and Ar–8%H_2 is almost identical at all temperatures. The shrinkage curves, under Ar and Ar–8%H_2 atmospheres, superimpose one over the other as shown in Fig. 3. But for UO_2–20%PuO_2, Ar was found to be a better medium for sintering than Ar–8%H_2. For all the other compositions, shrinkage was found to be faster in Ar–8%H_2 than Ar. From the shrinkage rate curves, it was observed that the maximum shrinkage rate occurs for commercial N_2 atmosphere for UO_2 and UO_2–50%PuO_2. For other composition, the maximum shrinkage rate was observed for Ar atmosphere. For the pellets sintered in Ar–8%H_2, especially for PuO_2, large oscillations were noticed above 1100°C in $\mathrm{d}(\mathrm{d}l/l_0)/\mathrm{d}t$ curves. The same type of observations have been noted for UO_2 and UO_2–76%PuO_2 in small magnitude.

The following conclusions can be drawn from the above observations:

1. UO_{2+x} was found to densify equally well in both Ar and Ar–8%H_2 atmospheres.
2. UO_2–20%PuO_2 pellet sinters slightly better in Ar than in Ar–8%H_2. But for pellets having higher PuO_2 content, Ar–8%H_2 was found to be more beneficial than Ar.
3. An expansion can be seen for UO_2–76%PuO_2 and PuO_2 in Ar atmosphere at around 1000°C.
4. Large oscillations were noticed in $\mathrm{d}(\mathrm{d}l/l_0)/\mathrm{d}t$ curves of PuO_2 sintered in Ar–8%H_2.
5. All pellets of the compositions covered in this study were found to sinter at much lower temperature in CO_2.

X-ray diffraction (XRD) pattern of UO_2, UO_2–20%PuO_2, UO_2–50%PuO_2, UO_2–76%PuO_2 and PuO_2 pellets sintered in CO_2 showed only single phase. But the diffraction pattern of the pellets with higher plutonium content such as UO_2–76%PuO_2 and PuO_2 pellets sintered in Ar–8%H_2 showed the presence of two phases-one is isostructural with PuO_2 and other is isostructural with bcc α-Pu_2O_3 (see Fig. 12). It was noticed that after sintering PuO_2 in Ar–8%H_2 at a temperature of 1500°C, 14 wt% PuO_2 got converted into bcc Pu_2O_3.

In the case of UO_2–76%PuO_2 pellet sintered in Ar–8%H_2, the shape of the peaks in the lower angle side indicate the presence of a phase isostructural with α-Pu_2O_3. Due to weak intensities of higher angle peaks, those peaks of α-Pu_2O_3 could not be observed. But scanning of UO_2–76%PuO_2 with 2θ rate 0.5°/min from 54.5° to 58° shows a partially overlapped (4 3 1) peak of a phase isostructural with bcc Pu_2O_3 phase. This is shown in Fig. 13. Lattice parameter of the major phase

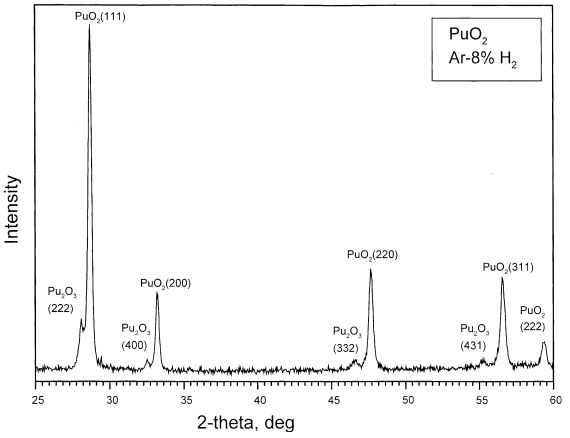

Fig. 12. XRD pattern of PuO_2 pellet sintered in Ar–8%H_2 atmosphere.

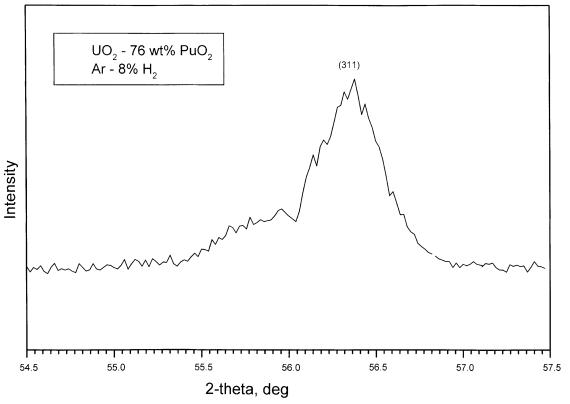

Fig. 13. XRD pattern of UO_2–76%PuO_2 in Ar–8%H_2 at slow scan rate.

i.e., (U,Pu)O_2 phase has been calculated to be 0.54049 nm which corresponds to PuO_2–13%UO_2 (according to Vegard's law). So, the rest of the UO_2 might have formed solid solution with Pu_2O_3 or formed mixed crystal of different composition with Pu_2O_3. A detailed explanation regarding the above phenomenon is given in Section 4.3.

4. Discussion

From the above results, it is clear that the shrinkage occurs more rapidly in oxidizing atmosphere. At 1100°C, the shrinkage was negligible for all compositions in Ar–8%H_2. On the other hand, shrinkage was quite appreciable in CO_2 medium at the above mentioned temperature, its value being highest for UO_2 (13%) and lowest for PuO_2 (6%).

Sinterability of UO_2–PuO_2 compacts has been found to depend upon the following factors, namely [15–19]:

1. Sintering temperature,
2. Sintering atmosphere,
3. Characteristics of the starting UO_2 and PuO_2 powders, and
4. Sintering time.

Sintering is a diffusion controlled process and is rate controlled by the slower moving metal atoms. Diffusion in solid itself occurs by jumps on an atomic scale via the movement of point defects. The point defect model has been used to explain many observed features of diffusion in non-stoichiometric fluorite type oxide fuels [1].

4.1. Point defect model

The point defect model was first developed by Matzke [1,8] and Lidiard [20]. They derived a relation for the temperature dependence of the concentration of vacancies and interstitials in both the oxygen and metal sublattice by solving the anion Frenkel, Schottky and cation Frenkel products. It has been shown that the activation enthalpy for metal diffusion should increase or decrease respectively, by ΔG_{FO} when passing from MO_2 to MO_{2+x} or MO_{2-x}, respectively, if the metal diffusion occurs via a vacancy mechanism, where ΔG_{FO} is the free energy of formation of oxygen Frenkel defects [2].

Deviations from stoichiometry produce point defects, most likely oxygen vacancies or metal interstitials in hypostoichiometric compounds and oxygen interstitials or metal vacancies in hyperstoichiometric compounds. The point defects are also created thermally in these materials, provided the temperature is high enough. These defects can exist as single, isolated point defects at low concentration. At higher concentrations, the defects will aggregate into clusters, will become ordered or will be eliminated by the formation of two or three dimensional defects such as dislocation loops, shear planes, voids etc. [21]. For the compounds like actinide oxides, the dominating defect species are often not rate controlling for diffusion dependent processes. In the fluorite structure, cation mobility is many orders of magnitude smaller than anion mobility. At 1400°C, D^O/D^U is found to be greater than 10^5 for UO_2 (depending on x) [22]. Cation diffusion coefficients are, therefore, difficult to measure. The plot of D^M as a function of O/M shows a minimum for D^M at an O/M value of ~1.98. The location of the minimum is found to be temperature dependent. Upon further reduction in O/M, D^M increases and subsequently reaches a saturation value when O/M~1.95. On increasing the O/M beyond 1.98, the D^M was found to increase drastically in hyperstoichiometric oxides because of a largely increased cation vacancy concentration. Because of their low mobilities, the diffusion of U and Pu is the rate determining step for many high temperature processes such as sintering, grain growth, precipitation etc. [2,7].

Interdiffusion coefficient D in UO_2–PuO_2 system strongly depends on the oxygen potential, Pu content and temperature [23]. It is well known that the tracer diffusion coefficient of U, D^U and of Pu, D^{Pu} in UO_{2+x} and MO_{2+x} vary by 4–5 orders of magnitude at constant temperature if the oxygen potential is varied [1,2]. Diffusion is slow under the reducing condition and it is fast under the oxidizing condition. The large increase in the diffusion values for hyperstoichiometric oxide is primarily due to the large metal vacancy concentration in the oxidized state, UO_{2+x} and MO_{2+x} [5,8,9]. At constant temperature, the metal defect concentration should depend on x^2. Elaborate work has been carried out by Matzke on MO_{2+x} and has predicted an x^2 dependence for metal self diffusion [1,2]. The expected strong dependence of D^M on x in MO_{2-x} was also confirmed by experiments on Pu in MO_{2-x} [2]. Three possible mechanisms are suggested for MO_{2-x} which are listed below [8,24,25]:

(a) A vacancy mechanism when O/M > 1.98,
(b) An interstitial mechanism for a lower O/M values (1.95 < O/M < 1.98),
(c) A cluster mechanism for O/M < 1.95.

4.2. Previous work on UO_2–PuO_2

There are many reports available in the literature regarding the sintering behaviour of UO_2–PuO_2 pellets in different atmospheres. The results of the these studies are often contradictory in nature. Chikalla [26] has studied the sintering behaviour of UO_2–PuO_2 pellets in different atmospheres and has observed that the physical addition up to 10% PuO_2 reduces the sinterability of UO_2 in H_2 atmosphere. A complete solid solution between UO_2 and PuO_2 occurs for both mixed and coprecipitated oxides on sintering in H_2. No PuO_2 has been found to be reduced in their study. Russell

et al. [27] have investigated the rate at which the solid solution was formed between UO_2 and PuO_2 and found the rate to be slow in H_2 than in Ar even at 1600°C. They reported that some of PuO_2 has been reduced to $PuO_{1.61}$ in H_2. Brett and Russell [15] have studied the sintering behaviour of UO_2–PuO_2 pellets in different atmospheres and reported the formation of a two phased microstructure for a composition containing more than 40% PuO_2 when sintered in H_2. The pellets sintered in H_2 at 1650°C for 3 h remained stoichiometric for composition between 0 and 60 mol% PuO_2. Akutsu et al. [16] have also reported a single phase for pellets of UO_2–40%PuO_2 sintered in N_2–5%H_2 mixture. A continuous series of solid solution between PuO_2 and UO_2 has been reported by Mulford and Ellinger [17]. Russell et al. [18] have fabricated UO_2–50%PuO_2 pellets and studied its sintering behaviour. They reported a single phase for the pellets sintered in Ar and in H_2 at 1650°C.

With this background in mind, we will discuss the effect of various atmospheres on the shrinkage behaviour of the UO_2, PuO_2, UO_2–20%PuO_2, UO_2–50%PuO_2 and UO_2–76%PuO_2 pellets. Based on Matzke's model, the metal vacancy concentration and metal interstitial concentration are calculated for the above compositions for oxidizing and reducing atmospheres and are shown in Table 3.

4.3. UO_2

UO_2 has been found to densify equally well in Ar and Ar–8%H_2. Since H_2O/H_2 ratio of Ar–8%H_2 sintering gas used in this study is less than 10^{-4}, a highly reducing environment is ensured inside the sintering furnace. The samples sintered in Ar and Ar–8%H_2 have almost identical O/M (see Table 3). This means that both have similar defect concentration which is found to be very low. Therefore, sintering commences only at a higher temperature of ~1100°C. On the other hand, the O/M of UO_2 sintered in CO_2 is around 2.100 which indicates that there are considerable amount of metal vacancies present in the system (see Table 3). At such large deviation from stoichiometry, the defects will aggregate into clusters.

During the sintering of UO_2, a prominent peak was observed in the shrinkage curve at around 400–600°C (see Fig. 3). This peak was observed only for UO_2 when the sintering was carried out in CO_2 atmosphere. The explanation for the appearance of this peak is as given below.

The UO_2 powder used for this study had an O/M ratio of 2.1 and hence the initial composition of the powder at room temperature should be $UO_2 + U_4O_{9-y}$ [5]. As the temperature increases, the surface oxidation of UO_2 takes place since CO_2 has high oxygen potential. The surface layers of the UO_2 is oxidized to U_3O_7. The formation of U_3O_7 has been reported during the slow heating of UO_2 in air [28]. The U_3O_7 is the intermediate product of oxidation of UO_2 before it is fully oxidised U_3O_8. The formation of U_3O_7 on the surface results in the formation of cracks. This results in the expansion which is manifested in the shrinkage curve at around 400°C. The formation of an intermediate oxide has also been reported by Matzke on heating UO_2 powder in CO_2 [1]. The formation of U_3O_8 results in a volume change of around 30% which may cause the pellet to disintegrate. Since no powder formation had been noticed during sintering in CO_2 atmosphere, it can be said that formation of U_3O_8 has not been occurred. Since U_3O_7 phase is not stable at high temperature, it decomposes to UO_{2+x}. The formation of UO_{2+x} from U_3O_7 results in a shrinkage. Therefore the net reaction occurring during the sintering of UO_2 in CO_2 atmosphere is the formation of U_3O_7 (which results in expansion) and decomposition of U_3O_7 (which results in contraction) to UO_{2+x}.

Role of O/U on sintering behaviour of UO_2 has been studied by Lay and Carter [29] and they have shown that U self diffusion coefficient in UO_{2+x} is proportional to x^2. D^U increases dramatically with x in UO_{2+x} at constant temperature (1700°C) by a factor of 10^5 between $UO_{2.00}$ and $UO_{2.20}$ [30–33]. This is predominantly due to the increased concentration of U vacancies in UO_{2+x}. From Table 3, it can be seen that the metal vacancy concentration is very high for UO_2 when sintered in CO_2 atmosphere. But at such large concentration, defects will aggregate into clusters.

Willis [34] has made detailed investigation of the defect structure of UO_{2+x} using Bragg neutron scattering technique. He found the evidence for two types interstitials, one (O′) displaced from (1/2,1/2,1/2) positions along $\langle 1\,1\,0\rangle$ axis and the other (O″) displaced along the $\langle 1\,1\,1\rangle$ axis. In addition to the excess oxygen, a significant number of adjacent normal oxygen atoms are displaced, thus creating an identical number of oxygen vacancies. On the basis of the above observation, Willis proposed a defect cluster containing two O′ interstitials, two O″ interstitials and two normal oxygen vacancies which is commonly known as 2:2:2 or Willis cluster. A more careful study of U sublattice indicates that U atoms are displaced somewhat by 0.25 A from their normal positions. Hence, oxygen diffusion will be drastically modified by the injection of vacancies and interstitials in UO_{2-x} and in UO_{2+x}. However, cation transport coefficient is also remain modified owing to the coupling of the Schottky and Frenkel disorder reaction, the effect of which is to enhance cation vacancies in the UO_{2+x} and suppress them in UO_{2-x}.

Therefore, a cluster mechanism is suggested for those pellets sintered in CO_2 and commercial N_2. On the other hand, a vacancy mechanism seems to be fitting for above composition when sintered in Ar and Ar–8%H_2.

4.4. PuO_2

The PuO_2 powder used in these experiments has a higher BET surface area than UO_2. Hence, PuO_2 is expected to sinter more readily than UO_2. However, this was not found to be true in all atmospheres. Our study has shown that PuO_2 sinters best in Ar–8%H_2 and least in CO_2.

Pritchard and Nance [35] have studied the sintering behaviour of PuO_2 in different atmospheres. They have reported that PuO_2 on sintering in Ar showed some reduction of PuO_2–Pu_2O_3 at around 1250–1350°C, and the amount of Pu_2O_3 increased with increase of temperature. For the pellet sintered in CO_2, no reduction of PuO_2 has been reported. PuO_2 has been found to sinter better in H_2 than in Ar and better in Ar than in CO_2. PuO_2 appears to sinter best in the temperature range of 1300–1600°C when O_2 pressure in the sintering atmosphere is maintained which ensures an O/M of 1.98–2.00. From the standard free energy of formation, an oxygen partial pressure of 3.6×10^{-3} atm is sufficient to stop the formation of Pu_2O_3 at 1650°C [35]. Chikalla [26] has reported that PuO_2 can be reduced to ~50% α-Pu_2O_3 on heating in H_2 at 1650°C or to 25%Pu_2O_3 on just heating at 1450°C. PuO_2 loses little amount O_2 on heating up to 1100–1200°C in inert or reducing atmosphere but loses O_2 readily at high temperature [36]. The oxygen deficiency results in the formation of large of Pu^{+3} ion which causes the unit cell to expand.

The superior sintering behaviour of PuO_2 in Ar–8%H_2 observed in this study may be associated with the presence of defect structure as PuO_2 gets reduced to Pu_2O_3. This has been confirmed by XRD analysis. In CO_2, sinterability of PuO_2 was found to be poor. This may be due to the fact that PuO_2 remains PuO_2 throughout the sintering temperature due to the high oxidizing potential of CO_2 medium. Since, no defects are generated, diffusion becomes low and this results in poor sintering behaviour. PuO_2 sinters better in Ar than in CO_2 because at high temperature PuO_2 loses its stoichiometry and becomes PuO_{2-x}. This defect structure enhances its sintering behaviour. Our results has been found agree with the earlier observations reported on PuO_2.

The formation of Pu_2O_3 during the sintering results in the expansion of the unit cell. The expansion in the shrinkage curves at around 900–1100°C may be thus attributed due to the formation of Pu^{+3} ion. Also Pu^{+3} ion can move faster than Pu^{+4} ion since it has a low migration energy resulting a faster diffusion (see Table 4). Therefore formation of Pu_2O_3 in the sample helps in achieving a faster shrinkage rate.

From the above discussion, the mechanisms suggested for the sintering of PuO_2 for oxidizing and reducing atmospheres are vacancy and cluster mechanisms, respectively. As described earlier, point defect models fail to describe the defect structure of oxide if the degree of non-stoichiometry is large enough. Because of their charges, point defects tend to cluster at higher concentration as a result of Coulomb interaction. These defects will become ordered or will get eliminated by the formation of two- or three-dimensional defects such as shear planes, dislocation loops or voids. Cluster formation is well-known to occur in MO_{2-x} at large x values. The basic unit for such clusters in MO_{2-x} is a nucleus of known sesquioxide Pu_2O_3. The building unit for the clusters are thus of the type Pu^{+3}–V_O–Pu^{+3} where V_O is the oxygen vacancy.

Table 4
Ionic radii and migration energies of Pu and U ions

	Ionic radius (A)	Migration energy (eV)
U^{+4}	0.97	6.0
U^{+5}	0.87	7.32
U^{+6}	0.83	–
Pu^{+3}	1.08	4.11
Pu^{+4}	0.93	5.95

4.5. UO_2–76%PuO_2

UO_2–76%PuO_2 composition sinters to the highest density in Ar–8%H_2. This is due to the formation of Pu_2O_3 at high temperature which promotes sintering. In CO_2, although the shrinkage starts even at 600°C, it has not attained a higher density even at 1400°C because of high oxygen potential, where the stoichiometry is maintained and therefore less defects are present in the lattice. In Ar, up to 1400°C no shrinkage has occurred for this composition and an expansion is noticed in the shrinkage curves at around 1100°C. PuO_2 has decomposed to PuO_{2-x} and probably to Pu_2O_3 at this temperature in Ar.

XRD data indicate a two phased microstructure with the major phase being a solid solution of PuO_2–13%UO_2, the other phase being Pu_2O_3 in solid solution with UO_2. Similar observation has been reported by Russell et al. [27] in their study on UO_2–PuO_2 system. They have carried out a detailed phase analysis on UO_2 containing varying amounts of PuO_2 which is sintered in H_2 and reported the presence of a phase for higher UO_2–PuO_2 compositions (>60% PuO_2) which is similar to the one observed in this study. They suggested the formation of a solid solution between UO_2 and α-Pu_2O_3. The phenomenon of a solid solution formation between a fluorite type dioxide and C-rare earth sesquioxide has been reported by Brauer and Gradinger [37]. The criterion for solid solution for the above mentioned two oxides is that the difference between lattice parameter of fluorite type oxide and one half of the cell side of the sesquioxide should be less than 2.25%. The difference

between the lattice parameter of UO_2 and $a/2$ of α-Pu_2O_3 is only 0.6%. Hence, as per the above criterion, a solid solution between UO_2 and α-Pu_2O_3 is possible. The expansion observed in the shrinkage curve for Ar atmosphere was found to be higher than that for PuO_2 and may be accounted for the following phenomenon:

(a) Formation of large Pu^{+3} ions due to the reduction of PuO_2 to Pu_2O_3 at this temperature;

(b) Formation of large U^{+4} ion since some UO_{2+x} may be reducing to UO_2. Since U^{+4} ion is bigger than U^{+5} and U^{+6} ions (Table 4) which results in further expansion of the lattice.

4.6. UO_2–50%PuO_2

Our experimental results shows that the O/M of $(U_{0.5}Pu_{0.5})O_2$ pellets sintered in Ar–8%H_2 and Ar is <1.97. At such a low O/M, an interstitial mechanism is suggested. Since O/M is below 1.90 for the pellets sintered in Ar–8%H_2, the major defects will be clusters. At O/M of 1.98, in a reducing atmosphere, the charge state of most of Pu will be Pu^{+3}. The Pu^{+3} ions were shown to diffuse faster than Pu^{+4} ions in ThO_2–PuO_2 system [2]. Also U^{+5} ion was found to diffuse more slowly than U^{+4} ion in UO_{2+x}. The migration energies for U^{+4} and Pu^{+4} are identical ($\sim$6eV) but the migration energy for U^{+5} is $\sim$22% higher and that for Pu^{+3} is about 31% lower than that of U^{+4} and Pu^{+4} (see Table 4).

Schmitz et al. [38] have given an alternate explanation for the observed increase in matter transport in MO_{2-x}. They have pointed out that two Pu^{+3} atoms connected to an oxygen vacancy would provide enhanced metal mobility via a type of ring mechanism [1].

Better shrinkage obtained in Ar–8%H_2 than Ar is due to large deviation of stoichiometry for pellets sintered in Ar–8%H_2 which enhances the sintering. In CO_2 and commercial N_2 atmosphere, the final O/M of the pellets is $\sim$2.0 (see Table 3). The CO/CO_2 ratio of the sintering gas is less than 10^{-4} ensuring a highly oxidizing atmosphere. Under such condition, Lidiard model [20] predicts a large increase in metal vacancy concentration and thus metal atom diffusion rates in hyperstoichiometric UO_{2+x}. This found to be true during oxidative sintering process in CO_2 or commercial N_2. Thus sintering under oxidizing condition with connected fast diffusion can be achieved in short time.

The data obtained in this study clearly indicate that UO_2–50%PuO_2 pellets can be fabricated in oxidizing atmosphere such as CO_2 or commercial N_2 at $\sim$1300°C whereas a temperature of more than 1650°C is required in Ar–8%H_2 atmosphere. The impurities in commercial N_2 ($\sim$500 ppm of O_2) helps in achieving faster shrinkage at around 1200°C [39]. N_2 has smaller ionic radius than CO_2 which helps in attaining a rapid shrinkage of $(U_{0.5}Pu_{0.5})O_2$ pellets in N_2 at around 1100°C.

4.7. UO_2–20%PuO_2

UO_2–20%PuO_2 pellets were found to sinter better in Ar than in Ar–8%H_2. This is expected since UO_{2+x} gets reduced to $UO_{2.0}$ in Ar–8%H_2 at higher temperature. But in Ar atmosphere, UO_{2+x} remains hyperstoichiometric even at higher temperature. Hence, more defects are present in pellet sintered in Ar resulting in better sintering behaviour of UO_2–20%PuO_2. The defects concentration from Table 3 indicates a large metal interstitial concentration. The increased diffusion of Pu in $(U,Pu)O_{2-x}$ at O/M < 1.98, may partly be due to faster mobility of Pu^{+3} ions. In CO_2 and commercial N_2, UO_2–20%PuO_2 sinters to the highest density even at a low temperature of 1300°C. This is because of the presence of large amount of metal vacancies. Since O/M of the pellet sintered in CO_2 and commercial N_2 is around 2.09, a cluster mechanism is the most probable. A Willis type clusters [34] are reported for UO_2 may be present in the system. Hence the mechanism for diffusion in UO_2–20%PuO_2 pellets in oxidizing and reducing atmospheres are cluster and metal interstitial mechanisms, respectively.

Another important point noticed during the densification is the retardation of shrinkage at around 800°C in Ar and Ar–8%H_2. The retardation of shrinkage correlates with the onset of the solid solution formation. The solid solution is formed by the interdiffusion of Pu^{+4} ion into UO_2 lattice and U^{+4} ion into PuO_2 lattice. These interdiffusion process decrease the sintering rate and shift shrinkage to a higher temperature. Such phenomenon has been reported for UO_2–30%PuO_2 and UO_2–Gd_2O_3 fuels [40,41]. The formation of solid solution of any actinide oxide will be difficult at around 800°C since they have high melting point of the order of 3000°C. But our study has clearly indicated that the shrinkage has occurred in CO_2 atmosphere at around 800°C. Fig. 11 shows that about 2.5% shrinkage has occurred at 800°C. This shows that some diffusion has occurred at that temperature. Our data are in agreement with those of Matzke. He has plotted density vs temperature for UO_2 in reducing and oxidizing atmosphere which clearly shows that there is no improvement in density in reducing atmosphere at 800°C. But in oxidizing atmosphere, the density has been really improved which is in agreement with our results.

Lay and Carter [29] have studied the influence of initial O/M ratio of UO_2 on its initial shrinkage rate in a given atmosphere using dilatometry. They calculated the values of diffusion coefficient in reducing and oxidizing atmospheres. In CO_2, the diffusion coefficient at 775°C was in the range of $0.5–12 \times 10^{-16}$ cm^2/s. And for H_2 atmosphere at 1250°C the value was in the range of $1–6 \times 10^{-16}$ cm^2/s. This shows that the value of diffusion coefficient for U cation is almost identical for CO_2 and H_2 atmospheres at 775°C and 1250°C, respectively,

Table 5
Standard point defect model of fluorite type oxides $MO_{2\pm x}$ and energies for different defect processes [1,42][a]

Defect concentrations	
Stoichiometric $MO_{2.00}$	$[V_M] = 2\exp[-(\Delta G_S - \Delta G_{FO})/kT]$
	$[M_I] = 0.5\exp[-(\Delta G_{FM} + \Delta G_{FO} - \Delta G_S)/kT]$
Hyperstoichiometric MO_{2+x}	$[V_M] = (4/x^2)\exp[-\Delta G_S/kT]$
	$[M_I] = (x^2/4)\exp[-(\Delta G_{FM} - \Delta G_S)/kT]$
Hypostoichiometric MO_{2-x}	$[V_M] = (4/x^2)\exp[-\Delta G_S/kT]$
	$[M_I] = (x^2/4)\exp[-(\Delta G_{FM} - \Delta G_S)/kT]$
Formation energies (eV)	
Oxygen Frenkel pair, ΔG_{FO}	3.5
Metal Frenkel pair, ΔG_{FM}	9.5
Schottky trio, ΔG_S	6.5
Migration energies (eV)	
Oxygen Vacancy, ΔH^m_{VO}	0.55
Oxygen interstitial, ΔH^m_{Oi}	0.9
Metal Vacancy, ΔH^m_{VM}	2.4
Metal interstitial, ΔH^m_{Mi}	8.76

[a] Metal = (Pu, U).

which once again suggests the advantage of oxidizing atmosphere for sintering.

5. Conclusions

The shrinkage behaviour of UO_2–PuO_2 compacts containing different amounts of PuO_2 were studied in Ar, Ar–8%H_2, CO_2 and commercial N_2 and the following conclusions are drawn:

1. Shrinkage begins at a much lower temperature in oxidizing atmosphere such as CO_2 and commercial N_2.
2. Shrinkage behaviour of UO_2 is almost identical in Ar and Ar–8%H_2.
3. PuO_2 and UO_2–76%PuO_2 showed an expansion on heating in Ar at ~1000°C.
4. UO_2–20%PuO_2 pellet was found to sinter better in Ar than Ar–8%H_2.
5. The shrinkage rate was found to be maximum in commercial nitrogen atmosphere for UO_2 and UO_2–50%PuO_2 while it was highest in Ar for UO_2–76%PuO_2 and PuO_2.

Acknowledgements

The authors are grateful to Dr A.K. Sengupta for his support during the course of this work. They are also thankful to Mr J.K. Ghosh, Dr G.C. Jain, Messers R. Keswani, T. Jarvis, K. Ravi, P. Sankaran Kutty, G.P. Mishra and S.K. Pal for their valuable support.

Appendix A

See Table 5.

References

[1] Hj. Matzke, in: T. Sorensen (Ed.), Non-Stoichiometric Oxides, Academic Press, New York, 1981, p. 156.
[2] Hj. Matzke, J. Nucl. Mater. 114 (1983) 121.
[3] P. Funke, W. Lins, V.W. Schneider, Fuel and Fuel Elements for Fast Reactors, IAEA, Vienna, 1974, p. 397.
[4] M. Coquerelle, Hj. Matzke, C.T. Walker, in: Proceedings of the IAEA Technical Committee Meeting on Recycling of Plutonium and Uranium in Water Reactor Fuels, paper no.23, Cadarache, 13–16 November 1989.
[5] C.R.A. Catlow, J. Chem. Soc. Faraday Trans. 2 (1987) 1065.
[6] R. Thiessen, D. Vollath, Plutonium as a Reactor Fuel, IAEA, Vienna, 1967, p. 253.
[7] Hj. Matzke, Philos. Mag. A 64 (1991) 1181.
[8] Hj. Matzke, J. Chem. Soc. Faraday Trans. 83 (1987) 1121.
[9] J.R. Mathews, J. Chem. Soc. Faraday Trans. 83 (2) (1987) 1273.
[10] E.R. Gardner, T.L. Markin, R.S. Street, J. Inorg. Nucl. Chem. 27 (1965) 541.
[11] H.A. Wriedt, Bull. Alloy Phase Diagram 11 (1990) 184.

[12] C.R.A. Catlow, in: T. Sorensen (Ed.), Non-stoichiometric Oxides, Academic Press, New York, 1981, p. 61.
[13] P. Jean-Baptiste, French Report CEA-R-5139, 1981.
[14] D.R. Olander, Fundamental aspects of nuclear reactor fuel elements, TID-26711-P1, US Department of Energy, 1976, p.145.
[15] N.H. Brett, L.E. Russell, Atomic Energy Research Establishment, Harwell Report, AERE-R 3900, 1962.
[16] H. Akutsu, K. Yoshioka, Y. Nakamura, Plutonium as a reactor fuel, IAEA, Vienna, 1967, p. 335.
[17] R.N.R. Mulford, F.H. Ellinger, J. Am. Chem. Soc. 80 (1958) 2023.
[18] L.E. Russell, N.H. Brett, J.D.L. Harrison, J. Williams, J. Nucl. Mater. 5 (1962) 216.
[19] T.D. Chikalla, Hanford atomic products operation report, Richland, Washington, HW-63081, 1959.
[20] A.B. Lidiard, J. Nucl. Mater. 19 (1966) 106.
[21] G.E. Murch, C.A. Catlow, J. Chem. Soc. Faraday Trans. 83 (2) (1987) 1157.
[22] Hj. Matzke, J. Phys. 34 (1973) 317.
[23] Hj. Matzke, J. Chem. Soc. Faraday Trans. 86 (1990) 1243.
[24] M. Aybers, J. Nucl. Mater. 226 (1995) 27.
[25] M.El. Sayad Ali, O.T. Sorensen, J. Therm. Anal. 25 (1982) 175.
[26] T.D. Chikalla, Hanford atomic production operation report, Richland, Washington, HW-60276, 1959.
[27] L.E. Russell, N.H. Brett, J.D.L. Harrison, J. Williams, A.G. Adwick, Atomic Energy Research Establishment, Harwell Report, AERE-R-3519, 1960.
[28] P.A. Tempest, P.M. Tucker, J.W. Taylor, J. Nucl. Mater. 151 (1988) 251.
[29] K.W. Lay, R.E. Carter, J. Nucl. Mater. 30 (1969) 74.
[30] Hj. Matzke, R.A. Lambert, J. Nucl. Mater. 64 (1977) 211.
[31] M.H. Rand, T.L. Markin, Thermodynamics of Nuclear Materials, IAEA, Vienna, 1967, p. 637.
[32] D. Glasser-Leme, Hj. Matzke, Solid State Ionics 12 (1984) 217.
[33] G. Riemer, H.L. Scheriff, J. Nucl. Mater. 39 (1971) 183.
[34] B.T.M. Wills, Acta Crystallogr. 18 (1965) 75.
[35] W.C. Pritchard, R.L. Nance, Los Alamos Report, Los Alamos, LA-3493, 1965.
[36] T.D. Chikalla, C.E. McNeilly, R.E. Skavdahl, J. Nucl. Mater. 12 (1964) 131.
[37] G. Brauer, H. Gradinger, Z. Anorg. u. Allg. Chem. 276 (5&6) (1954) 209.
[38] F. Schmitz, A. Marajofsky, Thermodynamics of Nuclear Materials, IAEA, Vienna, 1975, p. 467.
[39] T.R.G. Kutty, P.V. Hegde, R. Keswani, K.B. Khan, S. Majumdar, D.S.C. Purushotham, J. Nucl. Mater. 264 (1999) 10.
[40] R. Manzel, W.D. Dorr, Bull. Am. Ceram. Soc. 59 (1980) 601.
[41] W. Dorr, S. Hellmann, G. Mages, J. Nucl. Mater. 140 (1986) 7.
[42] Hj. Matzke, Atomic Energy Canada Ltd, Report AECL – 2585, 1966.